



Assessment of the breakup of the Antarctic polar vortex in two new chemistry-climate models

M. M. Hurwitz,^{1,2} P. A. Newman,¹ F. Li,³ L. D. Oman,^{1,4} O. Morgenstern,^{5,6} P. Braesicke,⁶ and J. A. Pyle⁶

Received 6 July 2009; revised 4 November 2009; accepted 11 November 2009; published 14 April 2010.

[1] Successful simulation of the breakup of the Antarctic polar vortex depends on the representation of tropospheric stationary waves at Southern Hemisphere middle latitudes. This paper assesses the vortex breakup in two new chemistry-climate models (CCMs). The stratospheric version of the UK Chemistry and Aerosols model is able to reproduce the observed timing of the vortex breakup. Version 2 of the Goddard Earth Observing System (GEOS V2) model is typical of CCMs in that the Antarctic polar vortex breaks up too late; at 10 hPa, the mean transition to easterlies at 60°S is delayed by 12–13 days as compared with the ERA-40 and National Centers for Environmental Prediction reanalyses. The two models' skill in simulating planetary wave driving during the October–November period accounts for differences in their simulation of the vortex breakup, with GEOS V2 unable to simulate the magnitude and tilt of geopotential height anomalies in the troposphere and thus underestimating the wave driving. In the GEOS V2 CCM the delayed breakup of the Antarctic vortex biases polar temperatures and trace gas distributions in the upper stratosphere in November and December.

Citation: Hurwitz, M. M., P. A. Newman, F. Li, L. D. Oman, O. Morgenstern, P. Braesicke, and J. A. Pyle (2010), Assessment of the breakup of the Antarctic polar vortex in two new chemistry-climate models, *J. Geophys. Res.*, *115*, D07105, doi:10.1029/2009JD012788.

1. Introduction

[2] The breakup of the stratospheric polar vortices is associated with the onset of spring. In the Southern Hemisphere (SH), the weakening of the polar jet and transition from wintertime westerlies to summertime easterlies occurs during the September–October–November season [see, e.g., *Randel and Newman*, 1998]. The breakup of the polar vortices significantly impacts both chemistry and transport in the stratosphere [e.g., *Atkinson et al.*, 1989].

[3] Progress has been made in determining which factors affect polar vortex strength and persistence. Some studies have explored the relationship between polar vortex dynamics and polar ozone loss: *Shine* [1986] theorized that polar ozone loss cools the Antarctic lower stratosphere in late winter; more recent work [e.g., *Randel and Wu*, 1999] used observations to confirm this finding. Momentum deposition by gravity

waves decelerates the polar jets and may contribute to the breakup of the polar vortices in spring [e.g., *Limpasuvan et al.*, 2007]. Another stream of research has focused on the role of planetary wave driving on the breakup of polar vortices. *Waugh et al.* [1999] found that a late breakup of the Northern Hemisphere (NH) vortex was generally preceded by a period of anomalously weak eddy heat fluxes two months earlier; *Rao et al.* [2003] found a similar lagged anticorrelation between wave activity and the timing of final stratospheric warmings in the SH. Furthermore, the first observed midwinter warming of the Antarctic polar vortex in 2002 was associated with high planetary wave activity [see, e.g., *Kruger et al.*, 2005; *Newman and Nash*, 2005]. This evidence suggests that planetary wave driving is an essential component of the vortex breakup, and thus, planetary wave driving that is weak or ill-timed is likely to delay the final stratospheric warming.

[4] While most 3-D coupled chemistry-climate models (CCMs) can simulate the ozone hole, few CCMs can reproduce the observed timing of the vortex breakup. Specifically, the transition to easterlies at 60°S, a proxy for the timing of the vortex breakup, occurred later than observed in the majority of the CCM simulations of the late 20th century assessed by *Eyring et al.* [2006, Figure 2]. The delay in the mean date of the transition to easterlies exceeded a month in some CCMs, particularly in the lower stratosphere. CCMs, in which the transition to easterlies at 20 hPa was delayed as compared with observations, were given low “grades” for this diagnostic in the quantitative assessment by *Waugh and*

¹NASA Goddard Space Flight Center, Greenbelt, Maryland, USA.

²NASA Postdoctoral Program, Oak Ridge Associated Universities, Oak Ridge, Tennessee, USA.

³Goddard Earth Sciences and Technology Center, University of Maryland Baltimore County, Baltimore, Maryland, USA.

⁴Department of Earth and Planetary Sciences, Johns Hopkins University, Baltimore, Maryland, USA.

⁵National Institute of Water and Atmospheric Research, Omakau, New Zealand.

⁶NCAS–Climate–Chemistry, Department of Chemistry, University of Cambridge, Cambridge, UK.

Eyring [2008]. It is of scientific interest, and of interest to model developers, to better understand the differences between CCMs that perform relatively well or poorly with respect to the breakup of the polar vortices and to determine the causes of this common model deficiency.

[5] This paper assesses the breakup of the Antarctic polar vortex in two new CCMs. The CCMs are introduced in section 2. The seasonal cycles of temperature, zonal winds, and total ozone are shown in section 3.1. In section 3.2, the performance of both models is compared with the previous generation of CCMs, using the *Eyring et al.* [2006] transition to easterlies diagnostic; one model is able to capture the observed vortex breakup, while in the other model the vortex breakup is delayed. Furthermore, the strength of the 100 hPa heat flux in October and November is shown to diagnose the ability of a CCM to accurately simulate the vortex breakup. Section 3.3 examines the consequences of the delayed vortex breakup for temperature and the transport of trace species since existing evidence suggests that the poorly modeled breakup of the SH polar vortex in the Goddard Earth Observing System (GEOS) version 1 CCM biases other stratospheric diagnostics: *Stolarski et al.* [2006] reported that modeled positive ozone trends in the Antarctic middle stratosphere were offset by two to three weeks as compared with satellite observations of the phenomena. Section 4 summarizes the main findings.

2. Description of Models and Observational Data Sets

2.1. Meteorological Analyses

[6] The European Centre for Medium-Range Weather Forecasts' 40 year meteorological reanalysis (ERA-40) [*Uppala et al.*, 2005] is used to compare model results with observations. The ERA-40 data set has vertical coverage up to 1 hPa, and for this study, it is interpolated to a $2.5^\circ \times 2.5^\circ$ horizontal grid. Zonal wind, temperature, geopotential height, and eddy heat flux fields are shown in this work.

[7] The National Centers for Environmental Prediction–U.S. Department of Energy (NCEP–DOE) reanalysis-2 product [*Kanamitsu et al.*, 2002] is also included in the analysis of heat flux and vortex breakup date presented in section 3.2. NCEP reanalysis-2 has $2.5^\circ \times 2.5^\circ$ horizontal resolution with vertical coverage up to 10 hPa. The ERA-40 and NCEP reanalyses yield similar results for the 1980–2000 period.

2.2. GEOS V2

[8] Version 2 (V2) of the GEOS chemistry-climate model (hereafter GEOS V2) is based on the GEOS 5 atmospheric general circulation model (GCM). The horizontal resolution is the same as in the version 1 (V1) model ($2^\circ \times 2.5^\circ$). There are 72 vertical levels and a model top at 0.01 hPa. As described by *Rienecker et al.* [2008], the GEOS 5 GCM uses essentially the same advection and gravity wave drag schemes as the GEOS 4 GCM [*Bloom et al.*, 2005]. However, changes have been made to the physics parameterizations, such as the radiative transfer and convective components. The stratospheric chemistry component in GEOS V2 is essentially the same as in the GEOS V1 CCM; predicted distributions of

water vapor, ozone, greenhouse gases (CO_2 , CH_4 and N_2O), and CFCs (CFC-11 and CFC-12) feedback to the radiative calculations [see *Pawson et al.*, 2008].

[9] Section 3 considers the representation of the Antarctic vortex in V2 simulation P1. Similar to the GEOS V1 simulations assessed by *Pawson et al.* [2008], V2 P1 is a “reference past” run that attempts to reproduce the observed stratosphere. Specifically, V2 P1 is a “REF-B1” simulation (driven by annually varying emissions of ozone precursors, concentrations of ozone-depleting substances and greenhouse gases, sea surface temperatures (SSTs) and sea ice, spanning from 1960 through 2006), as defined by the Chemistry-Climate Model Validation (CCMVal) project [*Eyring et al.*, 2008]. Variability associated with the quasi-biennial oscillation (QBO), solar cycle, and volcanic eruptions is not considered.

2.3. UK Chemistry and Aerosols

[10] Like the GEOS V2 CCM, the stratospheric version of the UK Chemistry and Aerosols (UKCA) model is a new chemistry-climate model. This paper considers a “REF-B1” simulation of the recent past [see *Eyring et al.*, 2008].

[11] UKCA is based on the UK Met Office Unified Model 6.1 at $2.5^\circ \times 3.75^\circ$ horizontal resolution. The underlying GCM is nonhydrostatic, with 60 geometric height levels and a model top at approximately 84 km altitude. The UKCA model includes a detailed treatment of stratospheric chemistry. As for GEOS V2, water vapor, ozone, greenhouse gases (CO_2 , CH_4 and N_2O), and CFCs (CFC-11 and CFC-12) feedback to the model's dynamics [*Morgenstern et al.*, 2009]. The gravity wave drag parameterization follows *Scayfe et al.* [2002]. The setup and performance of the stratospheric version of UKCA in a perpetual 2000 simulation are described in detail by *Morgenstern et al.* [2009]. The stratospheric sensitivity of UKCA to high chlorine loading is discussed by *Morgenstern et al.* [2008].

3. Results

3.1. Simulation of Zonal Wind, Temperature, and Total Ozone in Two New CCMs

[12] This section provides an overview of the performance of GEOS V2 and UKCA in simulations of the recent past. The 1980–2000 mean seasonal cycles of zonal winds and temperature at 60°S , and SH total ozone fields, are shown for both of the CCM simulations in Figure 1. The ERA-40 reanalysis [*Uppala et al.*, 2005] and the Total Ozone Mapping Spectrometer (TOMS)/solar backscatter ultraviolet (SBUV) data set [*Stolarski and Frith*, 2006] are shown for comparison.

3.1.1. GEOS V2

[13] The observed annual cycles of zonal wind, temperature, and total ozone are generally well reproduced in GEOS V2. Upper stratospheric zonal winds in the Antarctic winter and the timing of the springtime transition to easterlies are poorly modeled (Figure 1b; see discussion in section 3.2). Despite a wintertime warm bias and summertime cold bias in the upper stratosphere, polar lower stratospheric temperatures, which are key to the correct simulation of the ozone hole, compare well with the ERA-40 reanalysis (Figures 1d–1f).

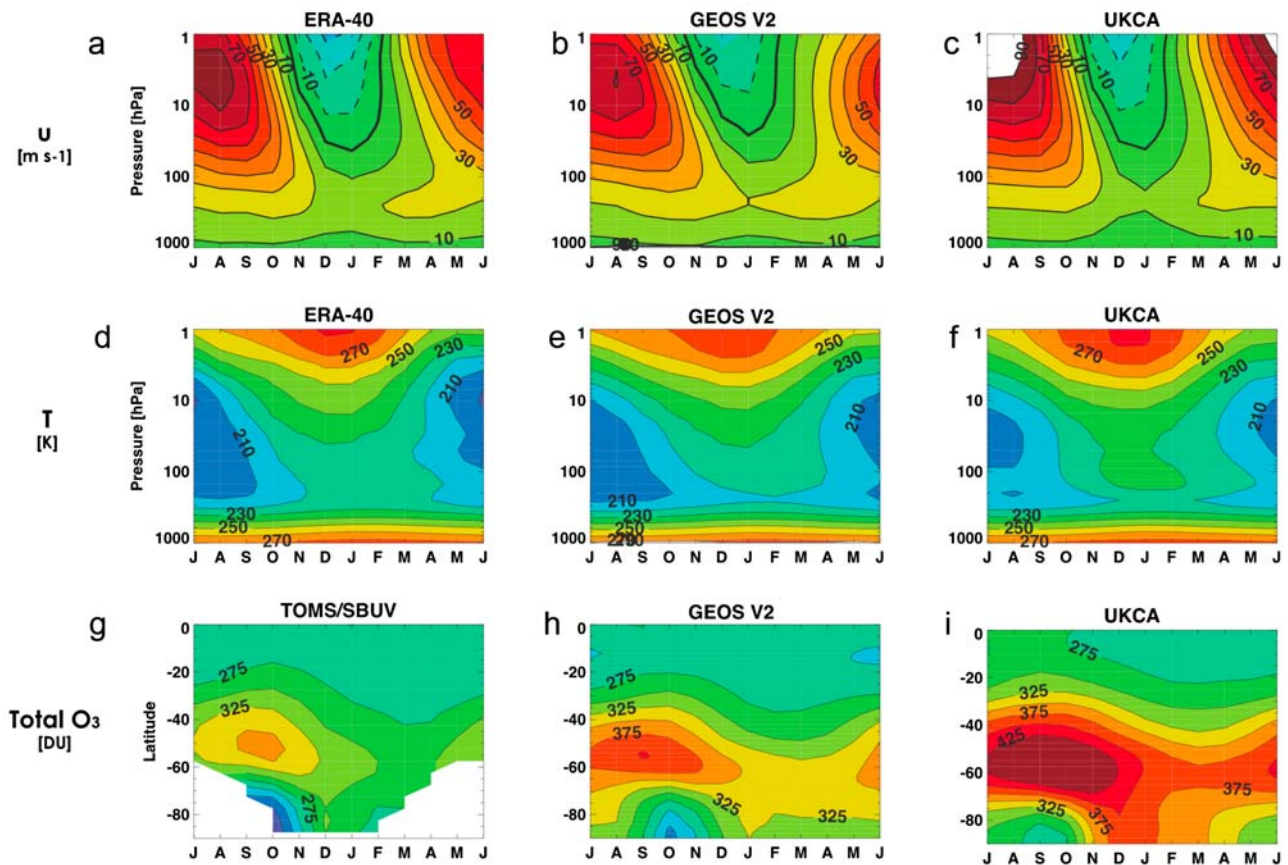


Figure 1. (a–c) Mean annual cycle of zonal mean zonal wind at 60°S (m s^{-1}), (d–f) temperature at 60°S (K) and (g–i) total ozone (DU), for the 1980–2000 period. (left) The observed mean fields (zonal wind and temperature from the ERA-40 reanalysis, TOMS/SBUV total ozone); (middle) mean fields from the GEOS V2 simulation; and (right) mean fields from the UKCA simulation. In Figures 1a–1c, the 0 m s^{-1} zonal wind contours are shown as the thick black lines.

[14] The ability of the GEOS V1 CCM to simulate the annual cycle of total ozone was discussed by *Eyring et al.* [2006]. They found that while most features of the observed total ozone field were well-reproduced by the V1 model, the middle-latitude ozone maximum in late winter/early spring was higher than detected by satellite instruments, associated with the stronger than observed SH polar jet, and in the 1990s the ozone hole was on average smaller than observed. These two model deficiencies worsened in GEOS V2; total ozone values are higher than observed both at midlatitudes in late winter and in the SH polar region in spring (Figure 1h).

3.1.2. UKCA

[15] For the recent past, observed stratospheric winds are well-reproduced by the UKCA CCM, though wintertime westerlies in the uppermost stratosphere are too strong (Figure 1c). The model has an internally generated quasi-biennial oscillation with a period of 4–5 years [*Morgenstern et al.*, 2009]. Stratospheric temperatures are generally well-simulated, though there is a warm bias at 100 hPa throughout the year at tropical latitudes (Figure 1f). Total ozone is well-simulated in the tropics, but similar to GEOS V2 (see Figure 1h) and to the CCMs discussed by *Eyring et al.* [2006], midlatitude total ozone is overestimated (Figure 1i).

3.2. Persistence of the Antarctic Polar Vortex and Relationship to Heat Flux

[16] This section aims to quantify the strength of the Antarctic polar vortex and the timing of the vortex breakup as represented in the GEOS V2 and UKCA CCMs.

[17] While the GEOS V2 CCM can in general simulate observed zonal winds (see Figures 1a and 1b), the modeled Antarctic vortex is too persistent. Differences between SH 10 hPa zonal mean zonal winds in GEOS V2 and the ERA-40 reanalysis, as a function of latitude and season, are highlighted in Figure 2c. Shown are the mean differences for the 1980–2000 period. The largest differences ($\sim 10 \text{ m s}^{-1}$ in the 70°S–50°S region) occur in November and December and are associated with the delayed breakup of the Antarctic vortex in GEOS V2. During the winter season (May through September), the modeled vortex is slightly weaker than observed. In UKCA (Figure 2e) the jet axis is positioned too far poleward (since the modeled polar vortex is too small [see *Morgenstern et al.*, 2009]); otherwise, 10 hPa zonal winds are well-simulated.

[18] Recent CCM comparison studies [e.g., *Austin et al.*, 2003; *Eyring et al.*, 2006] have used the modeled, meridional eddy heat flux at 100 hPa (equivalent to the vertical

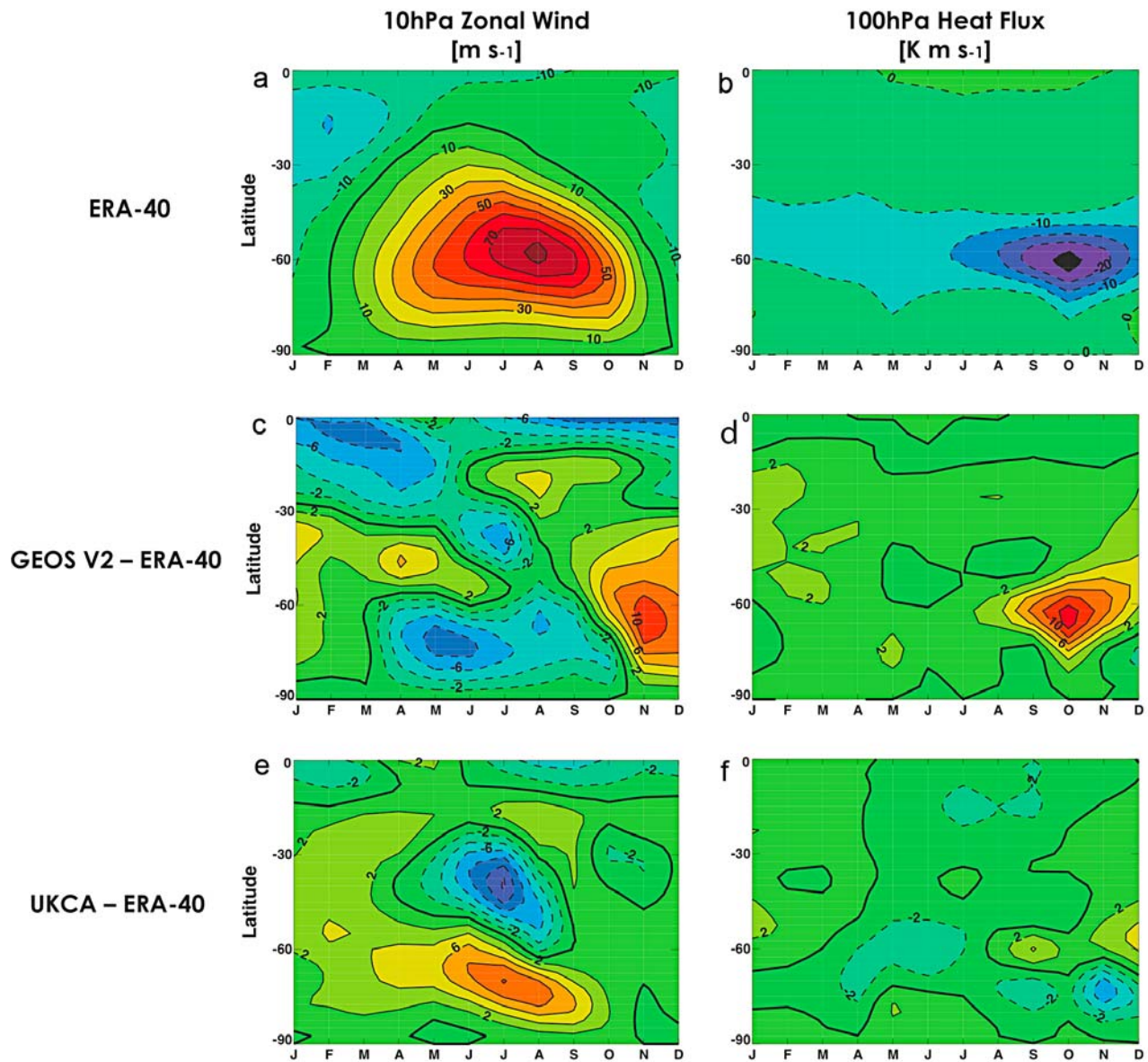


Figure 2. Annual cycles of 10 hPa zonal wind (m s^{-1}) and 100 hPa heat flux (K m s^{-1}), as a function of latitude, for the 1980–2000 period. (left) Zonal mean zonal wind at 10 hPa; (right) zonal mean eddy heat flux at 100 hPa. (a and b) ERA-40 mean fields; (c and d) differences between GEOS V2 and ERA-40; and (e and f) differences between UKCA and ERA-40.

component of the Eliassen–Palm flux [see *Andrews et al.*, 1987]) to diagnose planetary wave driving from the troposphere and evaluate the correlation between tropospheric forcing and high-latitude lower stratospheric temperature. As shown in Figure 2b, 100 hPa heat flux is negative (poleward) throughout the SH and is strongest at midlatitudes (40°S – 80°S) in October. The observed maximum in planetary wave driving corresponds with the location and timing where heat flux in GEOS V2 is too weak (i.e., positive differences peaking in October and November; see Figure 2d). Note that the period of weaker than observed heat fluxes precedes the period during which high-latitude winds are too strong by 1 month. Whereas the magnitude and seasonal

cycle of 100 hPa heat flux in UKCA compare well with the ERA-40 and NCEP means for 1980–2000 (see Figures 2f and 3); heat flux in GEOS V2 is too weak between September and November (as discussed in section 3.1). In GEOS V2, peak heat flux values occur in September rather than in October, as observed.

[19] Furthermore, the observed distribution of the 100 hPa heat flux between 1980 and 2000, in October and November, corresponds better with UKCA than with GEOS V2. Figure 4 shows histograms of the 100 hPa heat flux in July (Figures 4a, 4d, 4g, and 4j) October (Figures 4b, 4e, 4h, and 4k), and November (Figures 4c, 4f, 4i, and 4l) in the two CCM simulations, compared with the ERA-40 and NCEP

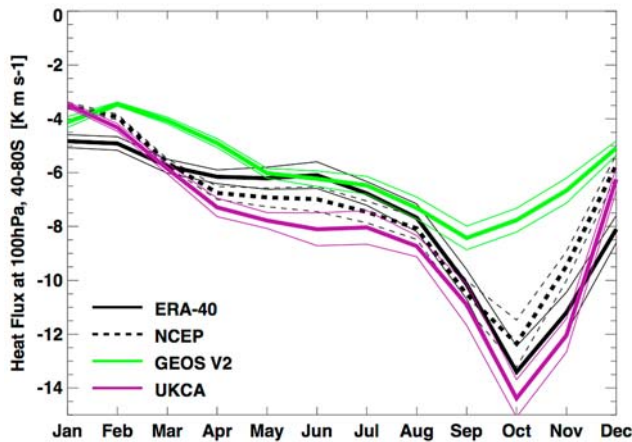


Figure 3. Annual cycle of the 1980–2000 mean eddy heat flux (K m s^{-1}) at 100 hPa, 40–80°S. The solid black line shows the ERA-40 reanalysis. The dashed black line shows the NCEP reanalysis. Also shown are the 1980–2000 mean annual cycles of eddy heat flux from the two simulations: GEOS V2 (green) and UKCA (purple). The thin lines indicate ± 1 standard error.

distributions; for reference, the dotted vertical lines show the 1980–2000 mean values in each case. The ERA-40 and NCEP means and distributions are similar in both July and October; in November, NCEP heat flux is weaker and less variable than in the ERA-40 reanalysis. The distribution of the heat flux values in the UKCA model (purple histograms) is in good agreement with the reanalysis distributions in all 3 months. The GEOS V2 CCM is able to reproduce the distribution of ERA-40 heat flux in July (and in other months; not shown), but in October and November the modeled heat flux is skewed toward the weak end of the ERA-40 and NCEP distributions.

[20] Because midlatitude heat flux in October and November appears to be an indicator of a CCM's ability to capture the strength of the polar stratospheric jet in November and December (see Figures 2, 3, and 4), the breakup of the Antarctic polar vortex is examined as a function of heat flux. In Figure 5, the timing of the transition to easterlies at 60°S, 10 hPa is shown as a function of October–November mean 100 hPa heat flux at midlatitudes (40°S–80°S). The stars show the date of the transition to easterlies in individual years, calculated from a smoothed time series of zonal winds at 10 hPa, as well as the October–November heat flux in individual years. The large diamond symbols indicate the mean heat flux values and breakup dates: On average the transition to easterlies occurs approximately 5 (4) days later in the UKCA model than in ERA-40 (NCEP) and approximately 13 (12) days later than ERA-40 (NCEP) in GEOS V2 (see Table 1). As has been previously mentioned in section 3.1 and this section, heat flux is significantly weaker in GEOS V2 than in either of the reanalyses. In Figure 5 the lines show the linear fit between October–November heat flux and the transition to easterlies. In each case, weaker heat flux leads to a later breakup of the polar vortex; all correlations exceed 0.60. The heat

flux-breakup date slopes are similar in the two reanalyses ($2.24 \pm 0.56 \text{ days}^{-1} \text{ K}^{-1} \text{ m}^{-1} \text{ s}$ in ERA-40 and $2.69 \pm 0.70 \text{ days K}^{-1} \text{ m}^{-1} \text{ s}$ in NCEP; see Table 1), steeper in UKCA ($3.37 \pm 0.79 \text{ days K}^{-1} \text{ m}^{-1} \text{ s}$) and steepest in GEOS V2 ($4.59 \pm 1.40 \text{ days K}^{-1} \text{ m}^{-1} \text{ s}$, for the 1980–2000 period).

[21] The mean delay in the breakup of the Antarctic polar vortex resulting from insufficient heat flux in GEOS V2 is similar to the mean delay in the breakup date related to ozone depletion [see *Akiyoshi et al.*, 2009]. In Figure 5 the heat flux-related delay (12–13 days) is shown as the difference between GEOS V2 for the 1980–2000 period (green stars and solid green line) and ERA-40 during this same period (black stars and solid black line). The ozone hole-related delay (~ 12 days) is approximated as the difference between the date of the transition to easterlies between 1980 and 2000 in GEOS V2 (green stars and solid green line) and the date of the transition to easterlies between 1961 and 1980 (green triangles and dot-dashed green line). The linear fits for 1961–1980 and 1980–2000 have nearly identical slopes (see Table 1). Note that the linear fit for the 1961–1980 period is not sensitive to the outlying heat flux value at $\sim -14 \text{ K m s}^{-1}$.

[22] Another way of representing the breakup of the Antarctic polar vortex as a function of heat flux is to examine the timing of the stratospheric transition to easterlies at 60°S when heat flux is particularly weak (low) or strong (high) (see Figure 6). Similar to Figure 2 of *Eyring et al.* [2006], the gray shaded area shows the range of variability of ERA-40 between 1980 and 2000. The black line indicates the mean date of the transition to easterlies in the ERA-40 reanalysis. (The mean date of the transition to easterlies is similar in the NCEP reanalysis and is therefore not shown; see Figure 5 and *Eyring et al.* [2006].) The solid green (purple) line indicates the mean transition date in the GEOS V2 (UKCA) model. The thin (thick) dashed lines indicate the average timing of the transition to easterlies in years when heat flux is more than one standard deviation lower (higher) than the 1980–2000 mean. As discussed above, UKCA is able to capture the observed timing of the vortex breakup whereas the modeled mean breakup date in GEOS V2 is somewhat later than in ERA-40 in the middle and lower stratosphere (specifically, a 12–13 day delay at 10 hPa). In the high heat flux case in ERA-40 and in both models, the transition to easterlies occurs at the early edge of the range of observed variability (late October at 1 hPa; early December at 30 hPa). In the ERA-40 low heat flux case, the transition to easterlies occurs at the late edge of the range of observed variability (mid-November at 1 hPa; late December at 30 hPa). In the GEOS V2 and UKCA low heat flux case the transition to easterlies is delayed by 2–3 weeks as compared with the ERA-40 mean. This suggests that it is the relative frequency of weaker than observed heat flux years in GEOS V2 that causes the mean transition to easterlies to lie outside the range of observed variability.

[23] Differences between the planetary wave driving in UKCA and GEOS V2 originate in the troposphere. Figure 7 shows longitude versus altitude maps of geopotential height deviations from the zonal mean at 60°S. The tilt and amplitude of zonal asymmetries in the geopotential height field determine the magnitude of the heat flux [*Holton*, 1979]. In Figure 7 the geopotential height deviations are

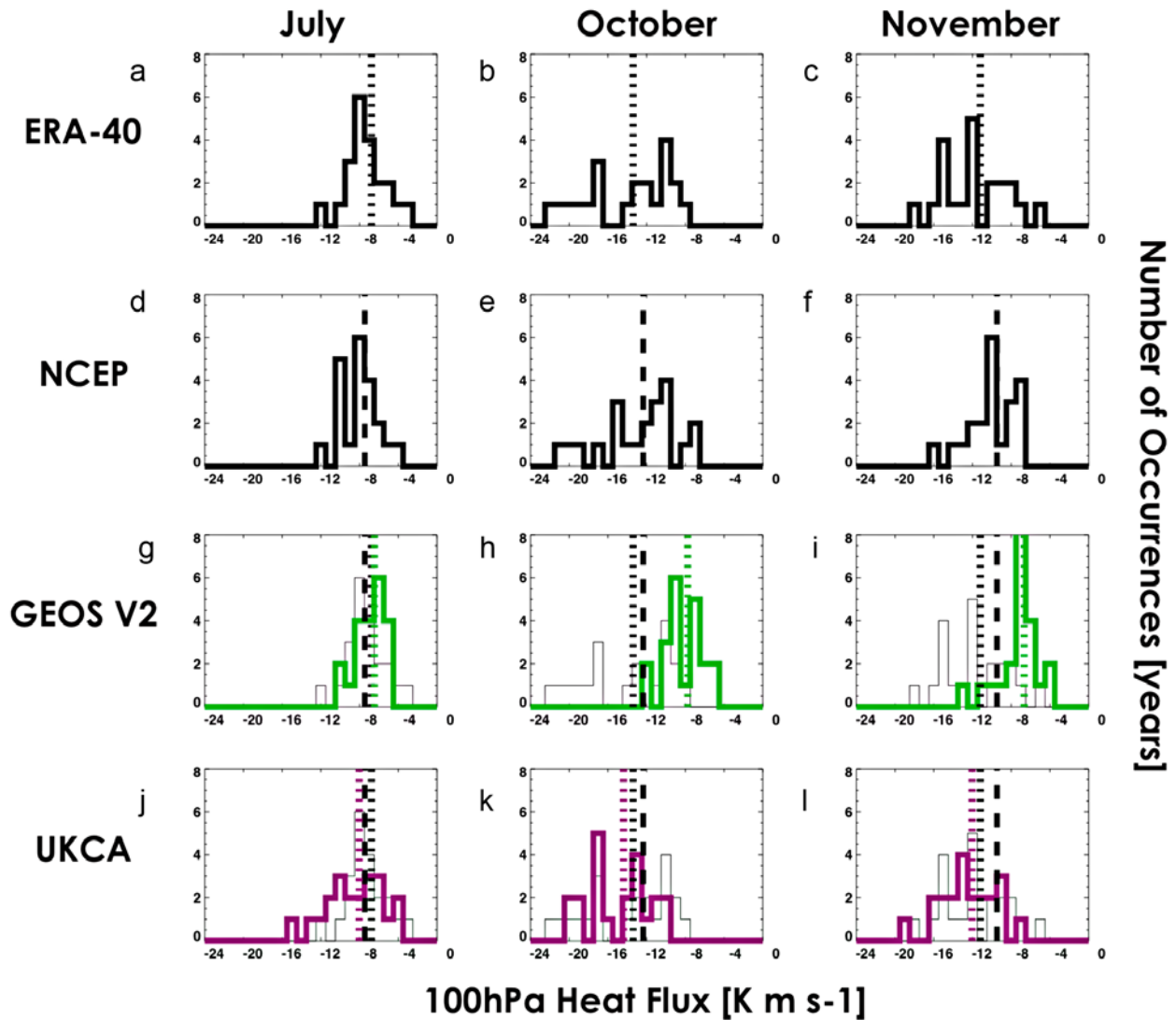


Figure 4. Histograms showing eddy heat flux (K m s^{-1}) at 100 hPa, 80° – 40° S for the 1980–2000 period in (left) July, (middle) October, and (right) November heat fluxes. (a–c) The distribution of heat flux magnitudes in ERA-40. (d–f) The distribution of heat flux magnitudes in the NCEP reanalysis. (g–l) The distribution of heat flux magnitudes in GEOS V2 (green) (Figures 4g–4i) and in UKCA (purple) (Figures 4j–4l); the ERA-40 distributions (black) are shown for reference in Figures 4g–4l. The vertical lines indicate the mean heat flux in each case: ERA-40 (black dotted), NCEP (black dashed), GEOS V2 (green dotted) and UKCA (purple dotted).

pressure-weighted to emphasize the wave structures in the troposphere and lower stratosphere. In July (Figures 7a, 7c, and 7e) the observed stationary wave pattern is well captured in both CCMs: both models have a prominent wave number 1 structure at 60° S. In October (Figures 7b, 7d, and 7f), while the tropospheric maximum is shifted approximately 50° west of the observed maximum, the midlatitude stationary wave pattern in UKCA is otherwise in agreement with ERA-40. In GEOS V2, wave number 2 dominates over wave number 1; note the separation between the two maxima at approximately 240° E. The stationary wave pattern is weaker than observed in the upper troposphere; in the stratosphere, the positive contours lack the westward tilt seen in ERA-40 and UKCA. (The November tropospheric wave

patterns are very similar to those in October and are therefore not shown.) Thus, the GEOS V2 model's lack of skill in reproducing the observed tropospheric stationary wave patterns in October and November corresponds with weaker than observed 100 hPa heat flux values during this same period.

3.3. Consequences of the Late Breakup of the Antarctic Polar Vortex in GEOS V2

[24] This section considers the consequences of the late breakup of the SH polar vortex on temperature, ozone, methane, and residual circulation in the middle atmosphere. Figure 8 shows differences between the mean low and high heat flux cases in the GEOS V2 simulation of the recent past. The analysis described below considers the 1961–

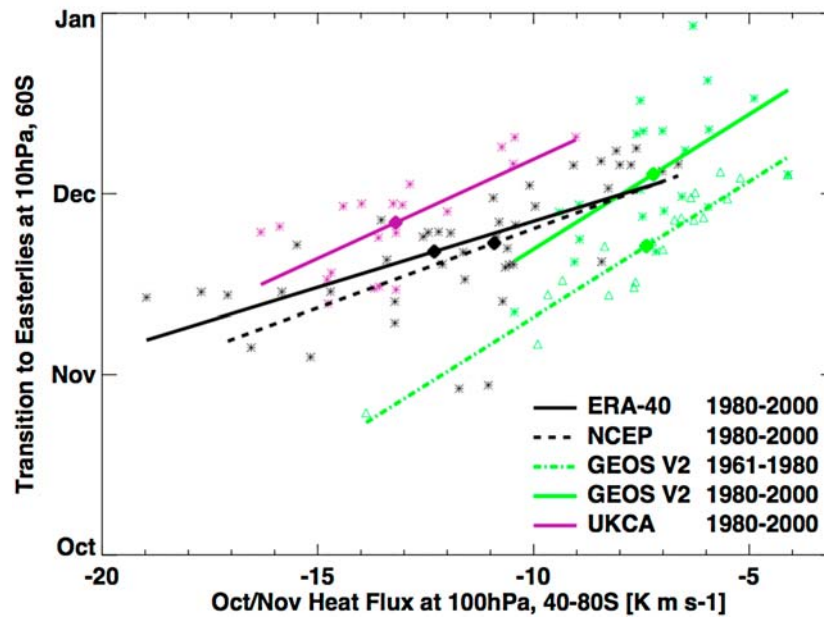


Figure 5. Scatterplot showing the date of the transition to easterlies at 10 hPa, 60°S as a function of the October–November mean heat flux (K m s^{-1}) at 100 hPa, 40–80°S. The ERA-40 (solid line) and NCEP (dashed line) reanalyses are shown in black. GEOS V2 is shown in green; UKCA is shown in purple. The linear fit for the 1980–2000 period is shown as the solid lines (the black dashed line in the case of NCEP), while stars indicate individual years. The dot-dashed green line (and green triangles) shows the linear fit for the 1961–1980 period in GEOS V2. The large diamonds indicate both the mean date of the transition to easterlies and the mean October–November heat flux value in each case.

2000 period, such that there are enough years when the 40°S–80°S, 100 hPa heat flux is at least one standard deviation higher than the 40 year mean (high) and lower than the 40 year mean (low) to allow differences between these two cases to be statistically significant. Figures 8a, 8c, 8e, and 8g show August–September fields based on heat flux in July–August; Figures 8b, 8d, 8f, and 8h show November–December fields based on heat flux in October–November. Figures 8a, 8b, and 8e–8h show percentage differences; white lines indicate the zero difference contour. The small (large) black crosses indicate percentage differences that are statistically significant at the 95% (99%) confidence level. In Figures 8e–8h (low–high differences for ozone and methane), gray dashed contours indicate the shape of the 1961–2000 mean fields. The streamlines (shown in

Figures 8c and 8d) indicate low–high differences in the residual circulation; the weight of the streamlines represents the magnitude of the circulation differences.

3.3.1. GEOS V2: August–September

[25] Previous work [e.g., *Newman et al.*, 2001; *Austin et al.*, 2003] has found 100 hPa heat flux to be positively correlated with 50 hPa polar temperatures in winter, with approximately a 1 month lag. Consequently, temperatures in the Antarctic stratosphere are higher in the high case than in the low case in midwinter (Figure 8a). This relative cooling (in years when heat flux is relatively lower) is statistically significant throughout the middle-latitude and high-latitude SH stratosphere; the weaker, positive low–high temperature differences seen in the tropical stratosphere are also statistically significant.

Table 1. Summary of the Relationship Between October–November Heat Flux Between 40°S and 80°S at 100 hPa and the Date of the Transition to Easterlies at 60°S, 10 hPa in the ERA-40 and NCEP Reanalyses, GEOS V2, and UKCA^a

Years	Mean October–November Heat Flux (K m s^{-1})	Mean Date of Transition to Easterlies (\pm days)	Delay as Compared with ERA-40 (days)	Slope of Heat Flux–Breakup Date Linear Fit ($\text{day s K}^{-1} \text{m}^{-1}$)	Heat Flux–Breakup Date Correlation
ERA-40	1980–2000	-12.30 ± 3.25	21 Nov (± 11)	2.24 ± 0.56	0.67
NCEP	1980–2000	-10.91 ± 2.62	23 Nov (± 11)	2.69 ± 0.70	0.66
GEOS V2	1961–1980	-7.38 ± 2.15	22 Nov (± 10)	4.60 ± 0.36	0.95
GEOS V2	1980–2000	-7.22 ± 1.53	4 Dec (± 12)	4.59 ± 1.40	0.60
UKCA	1980–2000	-13.22 ± 1.83	25 Nov (± 9)	3.37 ± 0.79	0.71

^aThis relationship is illustrated in Figure 5. The mean date of the transition to easterlies has been rounded to the nearest day. Bold values indicate statistically significant differences from ERA-40. All correlation coefficients are statistically significant at the 99% confidence level.

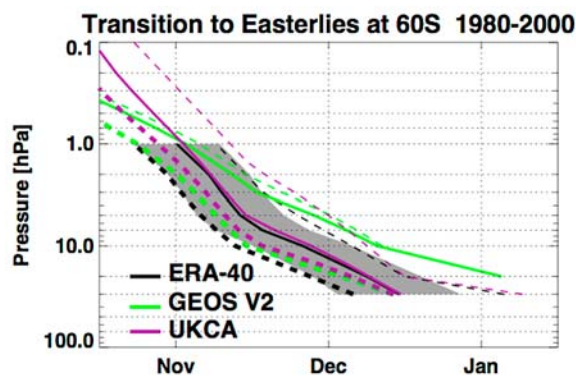


Figure 6. Timing of the transition to easterlies at 60°S during the 1980–2000 period, as a function of altitude (similar to Figure 2 of *Eyring et al.* [2006]). The black line shows the mean date of the transition from westerlies to easterlies for the ERA-40 reanalysis data set; the gray shading indicates the range of variability between 1980 and 2000. The solid lines (green, GEOS V2; purple, UKCA) show the simulated mean date of the transition to easterlies between 1980 and 2000. The thick (thin) dashed lines show the mean date of the transition to easterlies in cases when the 100 hPa heat flux between 40°S and 80°S is high (low).

[26] Lower polar stratospheric temperatures are associated with weakened downwelling at high latitudes. In GEOS V2, the low-high differences in the overturning circulation have a reversed Brewer-Dobson-like structure: streamlines show a relative ascent of air at high latitudes, equatorward transport through the middle atmosphere, and descent at low latitudes (Figure 8c). That the meridional overturning circulation is stronger when 100 hPa heat fluxes are high is expected since planetary-scale waves drive the Brewer-Dobson circulation.

[27] Consistent with the low-high differences in the residual circulation are differences in ozone and methane. At low latitudes, the weaker circulation transports less ozone to the upper stratosphere, increasing ozone concentrations in the tropical lower stratosphere. The relatively weaker downwelling at high latitudes means that ozone concentrations at $\sim 60^{\circ}\text{S}$ are relatively higher in the upper stratosphere (3–5 hPa; ozone-mixing ratio differences exceed 2 ppmv in this region) but relatively lower in the middle stratosphere (10–50 hPa; Figure 8e). Similarly, because of the weakened Brewer-Dobson circulation, relatively less methane is transported from low latitudes to the polar upper stratosphere, and the normally methane-poor air from this region is transported downward to regions of relatively higher-methane concentrations (Figure 8g). Thus, low-high methane differences are negative (and statistically significant) throughout the Antarctic stratosphere.

3.3.2. GEOS V2: November–December

[28] In November–December, negative low-high polar temperature differences (indicating areas where the 100 hPa heat flux is positively correlated with temperature) are restricted to the upper troposphere and lowermost stratosphere (Figure 8b). In the upper stratosphere, temperature differences are positive (and statistically significant). This

response is consistent with the filtering of wave activity by the polar vortex: in the high heat flux case in the upper stratosphere the polar vortex has broken down. Since wave activity cannot propagate into this region, as zonal winds are easterly, the polar upper stratosphere is close to its radiative equilibrium state. In the low heat flux case, however, wave activity can propagate up to the upper stratosphere, driving temperatures away from radiative equilibrium. Thus, in the SH spring, lower heat flux is associated with lower temperatures in the lower and middle Antarctic stratosphere (due to the persistence of the ozone hole) but with higher temperatures in the upper stratosphere.

[29] While the residual circulation in the lower stratosphere weakens in November–December, consistent with negative temperature differences, positive temperature differences in the polar upper stratosphere imply a strengthened circulation (an anticlockwise circulation cell, centered at 60°S ; Figure 8d). This circulation anomaly biases ozone transport and thus ozone-mixing ratios in the middle and upper Antarctic stratosphere: less ozone reaches the uppermost polar stratosphere (though negative differences are not statistically significant), while relatively more ozone is transported downward to the middle-latitude and high-latitude stratosphere (i.e., positive ozone differences poleward of 60°S at ~ 10 hPa; Figure 8f). Large, negative ozone differences in the lowermost polar stratosphere correspond with an increased capacity for ozone depletion in a relatively colder polar lower stratosphere. Furthermore, enhanced polar downwelling is consistent with negative low-high differences in methane near the SH pole (Figure 8h).

3.3.3. UKCA

[30] The low-high differences in temperature, residual circulation, ozone, and methane in UKCA (Figure 9) are qualitatively similar to those seen in GEOS V2. In August–September, temperature differences are negative at high latitudes and positive at low latitudes. In November–December, polar temperature differences are negative up to 10 hPa and positive above. Since high heat flux values are higher in UKCA than in GEOS V2 (see Figure 4) and thus low-high heat flux differences are generally larger in UKCA than in GEOS V2, the magnitudes of the low-high temperature differences are generally larger in UKCA.

[31] In August–September, as for GEOS V2, residual circulation differences represent a weakening of the Brewer-Dobson circulation. In November–December, the anticlockwise circulation cell centered at 60°S has a different shape to that seen in GEOS V2; this changes the relative transport of trace species in the Antarctic upper stratosphere. In UKCA, the strongest downwelling occurs near the pole, coincident with a maximum in positive ozone differences at 10 hPa; in GEOS V2 the polar downwelling maximizes at approximately 75°S , resulting in a relatively more equatorward position of the positive ozone maximum at 10 hPa.

[32] In UKCA, weaker than observed October–November heat flux years are balanced by stronger than observed heat flux years, and the breakup of the Antarctic vortex is not significantly delayed with respect to observations. Thus, the consequences of the delayed breakup described above do not apply to the UKCA model. However, the robustness of the low-high differences in GEOS V2 (Figure 8) and UKCA (Figure 9) implies that similar consequences would be

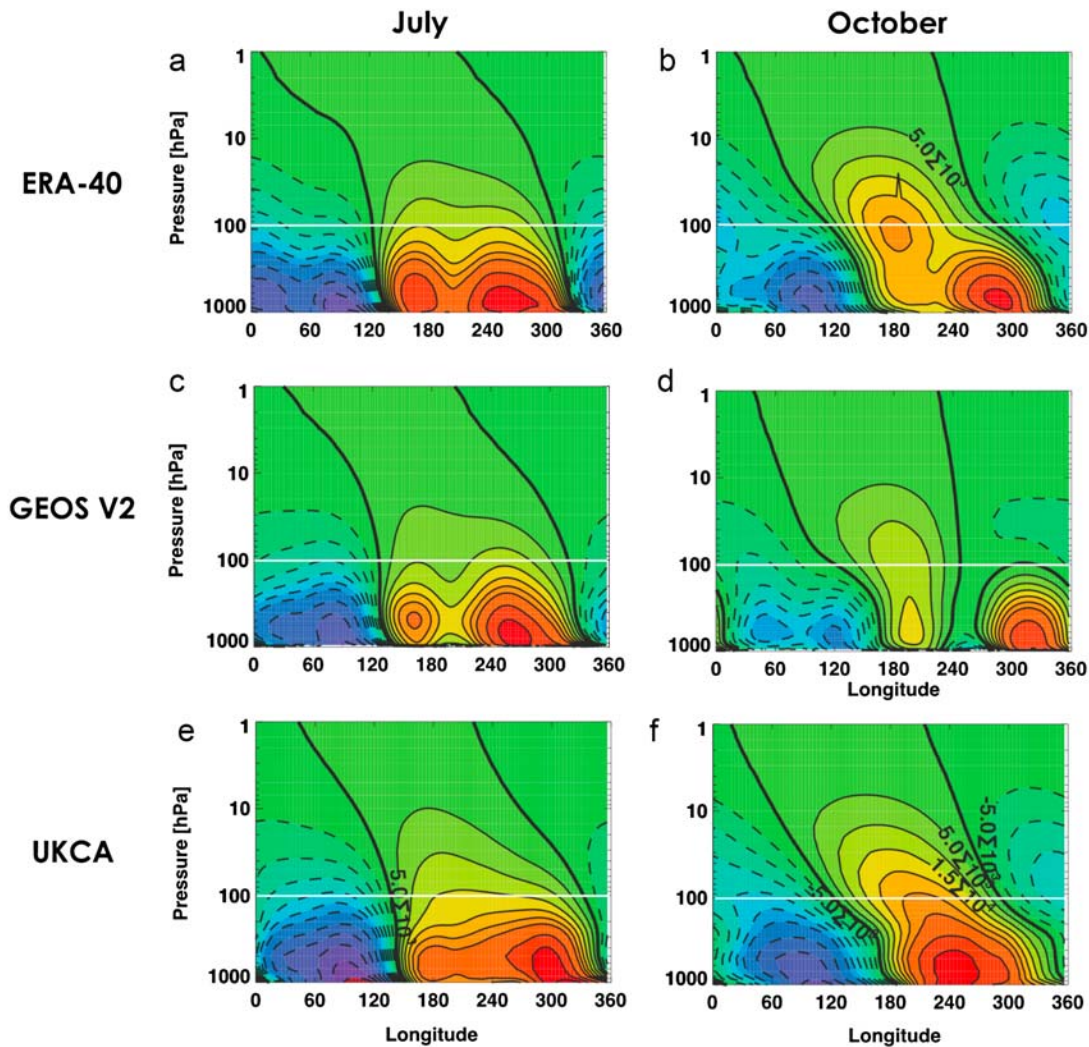


Figure 7. Tropospheric stationary wave patterns, at 60°S , for the 1980–2000 period, shown as the pressure-weighted geopotential height deviations from the zonal mean (m) in (left) July and (right) October for (a) ERA-40, (b) GEOS V2, and (c) UKCA. The 100 hPa level is indicated in white.

expected for other CCMs in which the breakup of the Antarctic vortex is delayed.

4. Discussion

[33] This paper assessed the timing of the breakup of the Antarctic polar vortex in two new chemistry-climate models (GEOS V2 and UKCA) and evaluated the consequences of the delayed vortex breakup in the GEOS V2 CCM.

[34] While both the GEOS V2 and UKCA CCMs can in general reproduce the stratospheric climate of the late 20th century (see Figure 1 and *Morgenstern et al.* [2009]), the two models perform differently with respect to the breakup of the Antarctic vortex. The vortex breakup was well-simulated in UKCA (the breakup occurred on average 5 days later than in ERA-40 and 4 days later than in the NCEP reanalysis at 10 hPa, though within the range of observed variability) but was delayed as compared with observations in GEOS V2. During the 1980–2000 period, the mean transition to easterlies at 10 hPa in GEOS V2

occurred approximately 13 (12) days later than in the ERA-40 (NCEP) reanalysis. The relatively better simulation of the vortex breakup in UKCA was associated with a warmer polar lower stratosphere and the overestimation of Antarctic total ozone (see Figure 1).

[35] This paper has shown that the timing of the Antarctic vortex breakup is related to the October–November middle-latitude heat flux at 100 hPa. Relatively strong heat flux is associated with earlier vortex breakup, while relatively weak heat flux delays the breakup. When heat flux is significantly weaker than observed in October and November, as in many years of the GEOS V2 simulation, the Antarctic vortex breaks down too late, and upper stratospheric zonal winds remain westerly during the November–December period (see Figures 2, 5, and 6). These same features can be seen in a subset of the CCMVal-1 models (as described by *Eyring et al.* [2005]).

[36] In the GEOS V2 model, insufficient heat flux in October–November has consequences for the dynamics and chemistry of the high-latitude SH stratosphere during

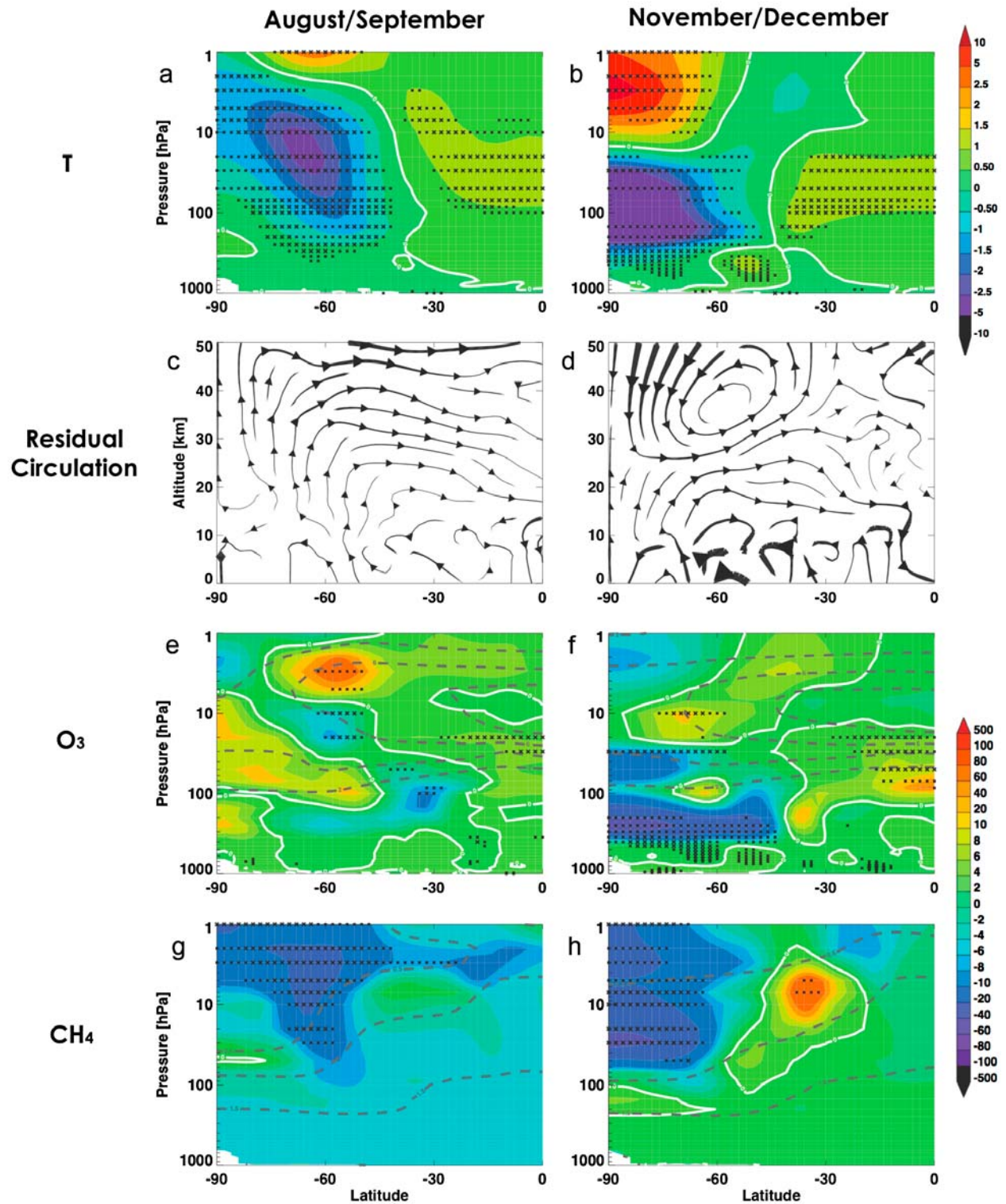


Figure 8. (a and b) Temperature (percentage differences), (c and d) residual circulation (streamlines), (e and f) ozone mixing ratio (percentage differences), and (g and h) methane mixing ratio (percentage differences) differences between the low and high heat flux cases in (left) August–September and (right) November–December for the GEOS V2 simulation. The white solid lines indicate the zero difference contours. The gray dashed contours in Figures 8e–8h indicate the simulated 1961–2000 mean ozone and methane fields (ppmv). The small black crosses indicate regions where low–high differences are significant at the 95% confidence level; the larger black crosses indicate regions where low–high differences are significant at the 99% confidence level.

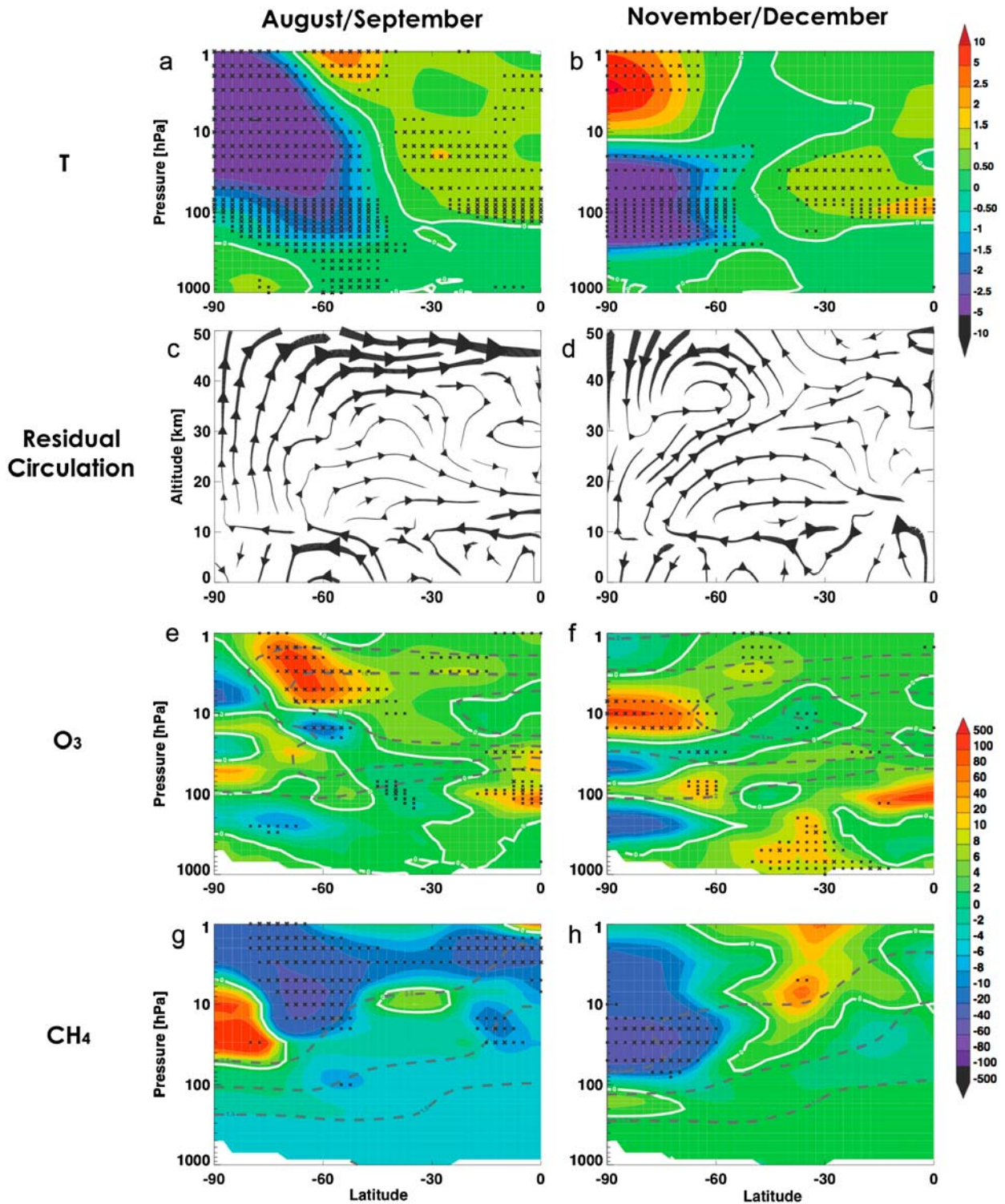


Figure 9. Differences between the low and high heat flux cases in (left) August–September and (right) November–December in the UKCA simulation. The same fields are shown and same the color scales are used as in Figure 8.

the austral spring season (see Figure 8): (1) In the late 20th century, unusually weak heat fluxes strengthened polar downwelling in the upper stratosphere; (2) upper stratospheric polar temperatures were too high; and (3) anomalous

circulation affected the distribution of trace species. Too little ozone was transported to the uppermost Antarctic stratosphere, while too much ozone was transported to the polar

Antarctic stratosphere at ~10 hPa. Too little methane was transported to the middle and upper Antarctic stratosphere.

[37] The ability of the two CCMs to simulate the observed tropospheric stationary wave structures (see Figure 7) was consistent with their ability to simulate 100 hPa heat flux, suggesting that the delayed breakup of the Antarctic vortex in GEOS V2 is the result of a tropospheric model deficiency. Recent work by I.-S. Song et al. (manuscript in preparation, 2010) has improved the distribution of gravity wave drag in the GEOS CCM from the Kiehl et al. [1998] and Garcia and Boville [1994] gravity wave drag schemes used in the GEOS V2 model (as described in this paper), yielding a realistic, internally generated QBO. However, these model improvements do not increase heat flux in the critical October–November period. Sensitivity simulations have determined that improving the distribution and magnitude of precipitation in the SH and doubling the model's horizontal resolution do improve the simulation of tropospheric stationary waves and thus of October–November heat flux. These findings will be examined in depth in a forthcoming paper.

[38] Thus, while it is beyond the scope of this paper to discuss how the breakup of the Antarctic polar vortex could be hastened in GEOS V2, the work presented in this paper does make it clear that this topic should be a priority for model developers. If GEOS V2 (and other models with similar problems simulating heat flux) cannot reproduce the observed persistence of the past and present Antarctic vortex, their skill in modeling the vortex under enhanced greenhouse gas concentrations (i.e., in the coming century) may be relatively low. A vortex that is too long-lived may increase the potential for ozone depletion because of the extended persistence of the ozone hole. Also, as this work has found, the delayed breakup of the SH vortex affects the middle-atmosphere circulation and thus, the distribution of ozone and other trace gases in the polar upper stratosphere in November and December; that is, the delayed breakup of the Antarctic polar vortex and its consequences hamper the ability of many of the present generation of chemistry-climate models to predict the strength of the Brewer-Dobson circulation and trace gas distributions in the Antarctic upper stratosphere in future.

[39] **Acknowledgments.** The authors thank the Chemistry-Climate Model Validation Activity (CCMVal) of World Climate Research Programme–Stratospheric Processes and their Role in Climate (WCRP–SPARC) for organizing the model data analysis activity. The UK MetOffice is acknowledged for use of the MetUM. Furthermore, the authors thank NASA's MAP program, E. Nash for providing the streamline plotting code, and J. E. Nielsen for running the GEOS V2 simulation. M. M. Hurwitz is supported by an appointment to the NASA Postdoctoral Program at Goddard Space Flight Center, administered by Oak Ridge Associated Universities through a contract with NASA. O. Morgenstern, P. Braesicke and J. A. Pyle are supported by the Natural Environmental Research Council through the NCAS initiative and by the European Commission under the Framework 6 SCOUT-O3 IP.

References

Akiyoshi, H., L. B. Zhou, Y. Yamashita, K. Sakamoto, M. Yoshiki, T. Nagashima, M. Takahashi, J. Kurokawa, M. Takigawa, and T. Imamura (2009), A CCM simulation of the breakup of the Antarctic polar vortex in the years 1980–2004 under the CCMVal scenarios, *J. Geophys. Res.*, *114*, D03103, doi:10.1029/2007JD009261.

Andrews, D. G., J. R. Holton, and C. B. Leovy (1987), *Middle Atmosphere Dynamics*, 489 pp., Academic, San Diego, Calif.

Atkinson, R. J., W. A. Matthews, P. A. Newman, and R. A. Plumb (1989), Evidence of the mid-latitude impact of Antarctic ozone depletion, *Nature*, *340*, 290–294, doi:10.1038/340290a0.

Austin, J., et al. (2003), Uncertainties and assessments of chemistry-climate models of the stratosphere, *Atmos. Chem. Phys.*, *3*, 1–27.

Bloom, S., et al. (2005), Documentation and validation of the Goddard Earth Observing System (GEOS) data assimilation system version 4, *Tech. Rep. 104606 V26*, NASA, Greenbelt, Md.

Eyring, V., D. E. Kinnison, and T. G. Shepherd (2005), Overview of planned coupled chemistry-climate simulations to support upcoming ozone and climate assessments, *SPARC Newslett.*, *25*, 11–17.

Eyring, V., et al. (2006), Assessment of temperature, trace species, and ozone in chemistry-climate model simulations of the recent past, *J. Geophys. Res.*, *111*, D22308, doi:10.1029/2006JD007327.

Eyring, V., M. P. Chipperfield, M. A. Giorgetta, D. E. Kinnison, E. Manzini, K. Matthes, P. A. Newman, S. Pawson, T. G. Shepherd, and D. W. Waugh (2008), Overview of the new CCMVal reference and sensitivity simulations in support of upcoming ozone and climate assessments and the planned SPARC CCMVal report, *SPARC Newslett.*, *30*, 20–26.

Garcia, R. R., and B. A. Boville (1994), “Downward control” of the mean meridional circulation and temperature distribution of the polar winter stratosphere, *J. Atmos. Sci.*, *51*, 2238–2245, doi:10.1175/1520-0469(1994)051<2238:COTMMC>2.0.CO;2.

Holton, J. R. (1979), *An Introduction to Dynamical Meteorology*, Academic, Orlando, Fla.

Kanamitsu, M., W. Ebisuzaki, J. Woollen, S.-K. Yang, J. J. Hnilo, M. Fiorino, and G. L. Potter (2002), NCEP–DOE AMIP-II Reanalysis (R-2), *Bull. Am. Meteorol. Soc.*, *83*, 1631–1643, doi:10.1175/BAMS-83-11-1631(2002)083<1631:NAR>2.3.CO;2.

Kiehl, J. T., J. J. Hack, G. B. Bonhan, B. A. Boville, D. L. Williamson, and P. J. Rasch (1998), The National Center for Atmospheric Research Community Climate Model: CCM3, *J. Clim.*, *11*, 1131–1149, doi:10.1175/1520-0442(1998)011<1131:TNCFA>2.0.CO;2.

Kruger, K., B. Naujokat, and K. Labitzke (2005), The unusual midwinter warming in the Southern Hemisphere stratosphere 2002: A comparison to Northern Hemisphere phenomena, *J. Atmos. Sci.*, *62*, 603–613, doi:10.1175/JAS-3316.1.

Limpasuvan, V., D. L. Wu, M. J. Alexander, M. Xue, M. Hu, S. Pawson, and J. R. Perkins (2007), Stratospheric gravity wave simulation over Greenland during 24 January 2005, *J. Geophys. Res.*, *112*, D10115, doi:10.1029/2006JD007823.

Morgenstern, O., P. Braesicke, M. M. Hurwitz, F. M. O'Connor, A. C. Bushell, C. E. Johnson, and J. A. Pyle (2008), The world avoided by the Montreal Protocol, *Geophys. Res. Lett.*, *35*, L16811, doi:10.1029/2008GL034590.

Morgenstern, O., P. Braesicke, F. M. O'Connor, A. C. Bushell, C. E. Johnson, S. M. Osprey, and J. A. Pyle (2009), Evaluation of the new UKCA climate-composition model—Part 1: The stratosphere, *Geosci. Model Dev.*, *2*, 43–57.

Newman, P. A., and E. R. Nash (2005), The unusual Southern Hemisphere stratosphere winter of 2002, *J. Atmos. Sci.*, *62*, 614–628, doi:10.1175/JAS-3323.1.

Newman, P. A., E. R. Nash, and J. E. Rosenfield (2001), What controls the temperature of the Arctic stratosphere during the spring?, *J. Geophys. Res.*, *106*, 19,999–20,010, doi:10.1029/2000JD000061.

Pawson, S., R. S. Stolarski, A. R. Douglass, P. A. Newman, J. E. Nielsen, S. M. Frith, and M. L. Gupta (2008), Goddard Earth Observing System chemistry-climate model simulations of stratospheric ozone-temperature coupling between 1950 and 2005, *J. Geophys. Res.*, *113*, D12103, doi:10.1029/2007JD009511.

Randel, W. J., and P. A. Newman (1998), The stratosphere in the Southern Hemisphere, in *Meteorology of the Southern Hemisphere*, edited by D. J. Karoly and D. G. Vincent, pp. 243–282, Am. Meteorol. Soc., Boston, Mass.

Randel, W. J., and F. Wu (1999), Cooling of the Arctic and Antarctic polar stratospheres due to ozone depletion, *J. Clim.*, *12*, 1467–1479, doi:10.1175/1520-0442(1999)012<1467:COTAAA>2.0.CO;2.

Rao, V. B., M. B. Rosa, J. P. Bonatti, and S. H. Franchito (2003), Stratospheric final warmings in the Southern Hemisphere and their energetics, *Meteorol. Atmos. Phys.*, *83*, 35–49, doi:10.1007/s00703-002-0558-6.

Rienecker, M. M., et al. (2008), The GEOS-5 data assimilation system—Documentation of versions 5.0.1, 5.1.0, and 5.2.0, in *Technical Report Series on Global Modeling and Data Assimilation*, NASA Tech. Memo., TM-2008-10460627.

Scaife, A. A., N. Butchart, C. D. Warner, and R. Swinbank (2002), Impact of a spectral gravity wave parameterization on the stratosphere in the Met Office Unified Model, *J. Atmos. Sci.*, *59*, 1473–1489, doi:10.1175/1520-0469(2002)059<1473:IOASGW>2.0.CO;2.

- Shine, K. P. (1986), On the modelled thermal response of the Antarctic stratosphere to a depletion of ozone, *Geophys. Res. Lett.*, *13*, 1331–1334, doi:10.1029/GL013i012p01331.
- Stolarski, R. S., and S. Frith (2006), Search for evidence of trend slowdown in the long-term (TOMS)/solar backscatter ultraviolet (SBUV) total ozone data record: The importance of instrument drift uncertainty, *Atmos. Chem. Phys.*, *6*, 4057–4065.
- Stolarski, R. S., A. R. Douglass, M. Gupta, P. A. Newman, S. Pawson, M. R. Schoeberl, and J. E. Nielsen (2006), An ozone increase in the Antarctic summer stratosphere: A dynamical response to the ozone hole, *Geophys. Res. Lett.*, *33*, L21805, doi:10.1029/2006GL026820.
- Uppala, S. M., et al. (2005), The ERA-40 re-analysis, *Q. J. R. Meteorol. Soc.*, *131*, 2961–3012, doi:10.1256/qj.04.176.
- Waugh, D. W., and V. Eyring (2008), Quantitative performance metrics for stratospheric-resolving chemistry-climate models, *Atmos. Chem. Phys.*, *8*, 5699–5713.
- Waugh, D. W., W. J. Randel, S. Pawson, P. A. Newman, and E. R. Nash (1999), Persistence of the lower stratospheric polar vortices, *J. Geophys. Res.*, *104*, 27,191–27,201, doi:10.1029/1999JD900795.
-
- P. Braesicke and J. A. Pyle, NCAS–Climate-Chemistry, Department of Chemistry, University of Cambridge, Lensfield Road, Cambridge CB2 1EW, UK.
- M. M. Hurwitz and P. A. Newman, NASA Goddard Space Flight Center, Code 613.3, Greenbelt, MD 20771, USA. (margaret.m.hurwitz@nasa.gov)
- F. Li, Goddard Earth Sciences and Technology Center, University of Maryland Baltimore County, 5523 Research Park Dr., Ste. 320, Baltimore, MD 21228, USA.
- O. Morgenstern, National Institute of Water and Atmospheric Research, Private Bag 50061, Omakau 9352, New Zealand.
- L. D. Oman, Department of Earth and Planetary Sciences, Johns Hopkins University, 301 Olin Hall, 3400 N. Charles St., Baltimore, MD 21218, USA.